Electronic Supplementary Material (ESI) for Chemical Science.
This journal is © The Royal Society of Chemistry 2023

Supporting Information for:

Multiexciton quintet state populations in a rigid pyrene - bridged parallel tetracene dimer

Liang-Chun Lin[a], Tanner Smith[b], Qianxiang Ai[b], Brandon K. Rugg[c], Chad Risko[b], John E. Anthony[b], Niels H. Damrauer[a,d], Justin C. Johnson[c,d].

a. Department of Chemistry, University of Colorado Boulder, Boulder, CO 80309, USA
b. Department of Chemistry & Center for Applied Energy Research, University of Kentucky, Lexington, Kentucky 40506-0055, USA.
c. National Renewable Energy Laboratory, 15013 Denver West Parkway, Golden, Colorado 80401, USA
d. Renewable and Sustainable Energy Institute (RASEI), University of Colorado Boulder; Boulder, CO, 80309, USA.

Synthesis

Synthetic details

All reagents were obtained from Sigma Aldrich, Alfa Aesar, Oakwood Chemical, or Geleste and used without further purification unless otherwise noted. Bulk solvents were obtained from VWR, while anhydrous, stabilizer free THF was purchased from Sigma-Aldrich. ^{1}H NMR spectra shown in Figure S17-S18 were measured on a 400 MHz Bruker NMR spectrometer in $CDCl_3$ (7.26 ppm). High resolution mass spectra (HRMS) were recorded using ESI as the ionization method. 2,7-di-t-butyl-4,5,9,10-tetrabromomethylpyrene **1**, 1-bromo-2,7-di-t-butyl-4,5-dibromomethylpyrene **3**, and NODIPS acetylene were prepared according to literature procedures[1,2]. Sonication was performed using a VWR Aquasonic P250HT. Crystal structures were collected and refined by Dr. Sean Parkin at the University of Kentucky-Department of

Chemistry using a dual-microsource Bruker D8 Venture κ-axis diffractometer (MoKα and CuKα) with large-area 'Photon-II' CMOS detector.

Step-by-step synthetic details for TPT

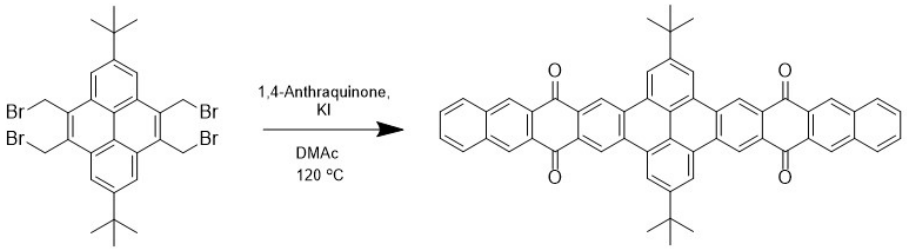

Synthesis of 2,7-di-t-butyl-4,5,9,10-pyrene bis(tetracenequinone) (2): A 150 ml sealed-tube reactor was charged with 50 ml of dimethylacetamide, and the solvent was purged with N_2 for 30 minutes. 2,7-di-t-butyl-4,5,9,10-tetra-bromomethyl pyrene **1** (1.20 g, 1.75 mmol), 1,4-anthraquinone (1.46 g, 7.00 mmol), and potassium iodide (2.91 g, 17.5 mmol) were added, the tube was sealed, and the mixture was stirred at 120 °C for two days. The mixture was cooled to room temperature, poured into 200 ml of water, then filtered. The recovered solid was added to 100 ml of acetone, sonicated for 10 minutes, and then filtered. The solid was then added to 100 ml THF, sonicated for 10 minutes, and filtered. The final crude product was recovered as a light brown solid. Yield: 1.1 g, 81%. The insoluble quinone was carried directly to the next step.

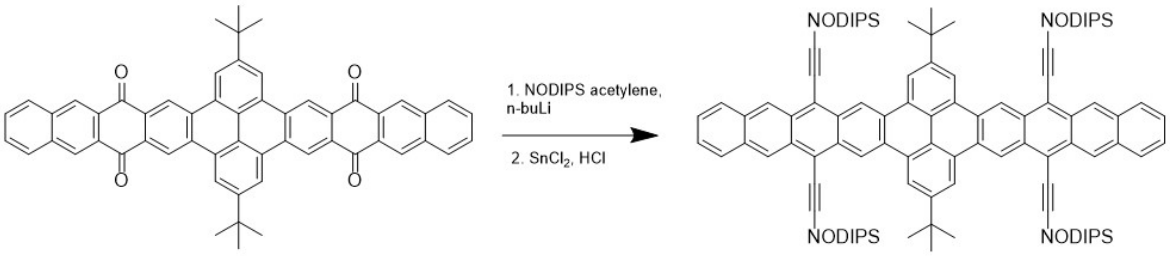

Synthesis of TPT: A flame-dried 100 ml round bottom flask under N_2 atmosphere was charged with 18 ml of hexanes and 9 ml of anhydrous THF. NODIPS acetylene (2.05 g, 8.12 mmol) was added and the solution was cooled to 0 °C. 2.5 M n-butyllithium in hexanes (3.09 ml, 7.72 mmol) was added slowly, and the solution was stirred for 1 hour. 2,7-di-t-butyl-4,5,9,10-pyrene bis(tetracenequinone) **2** (0.300 g, 0.387 mmol) was added, and the mixture was stirred overnight at room temperature. The mixture was quenched with water, and the organic layer was washed

with 10% aqueous HCl and water. The organic layer was dried with magnesium sulfate, and the organic layer was purified via silica plug in 5:1 hexanes:ethyl acetate. After the solvent was removed, the dark red oil was dissolved in THF, and $SnCl_2 \bullet 2H_2O$ (0.400 g, 1.77 mmol) dissolved in 2 ml 10% HCl was added dropwise, and the solution was stirred for 1 hr. The mixture was quenched with water, extracted into diethyl ether, dried with magnesium sulfate, and the solvent removed. The product was then purified by column chromatography in 10:1 Hexanes:DCM to give the product as a purple solid. Yield: 70.1 mg, 10.6%. ^{1}H NMR (400 MHz, CDCl3): δ 10.02 (s, 4H), 9.46 (s, 4H), 9.13 (s, 4H), 8.07 (dd, J = 7.2, 3.2 Hz, 4H), 7.51 (dd, J = 6.8, 3.0 Hz, 4H), 1.80 (s, 18H), 1.77 (m, 8H) 1.55 (m, 8H), 1.45 (m, 8H), 1.41 (m, 56H), 1.40 (m, 8H), 1.30 (m, 8H), 1.22 (m, 16H), 1.06 (m, 8H), 0.80 (t, J = 6.8 Hz, 12H). HRMS (APCI with direct probe injection) for [M+1]+: calc. For $C_{120}H_{162}Si_4$: 1715.1754, found: 1715.1798.

Step-by-step synthetic details for PT

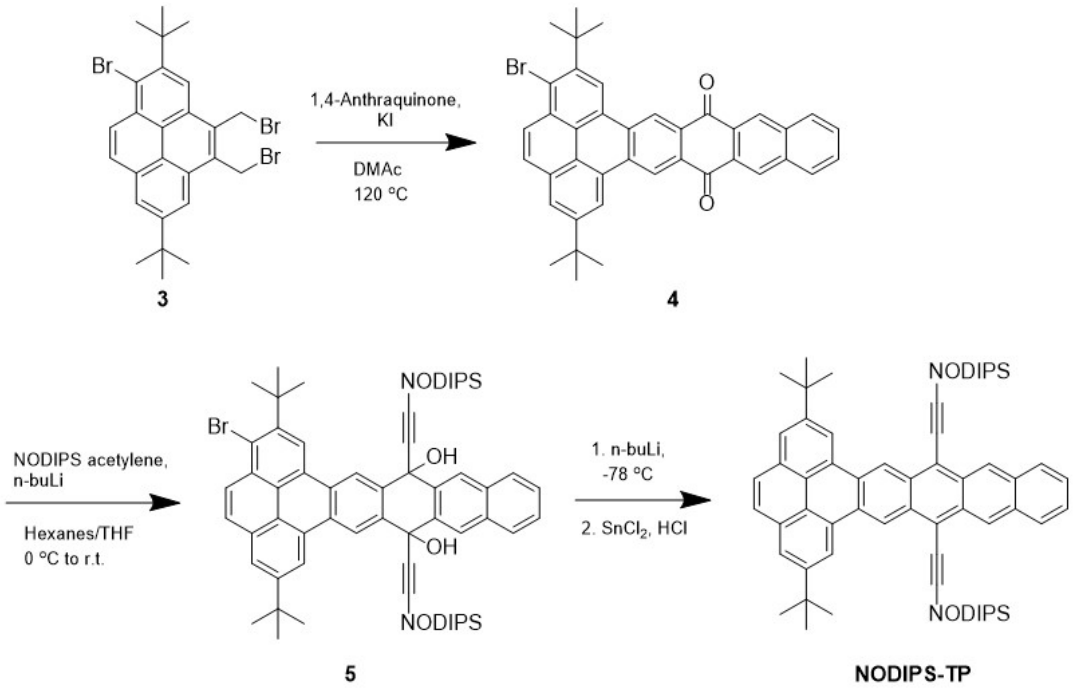

Figure S1. Synthesis scheme for **PT**.

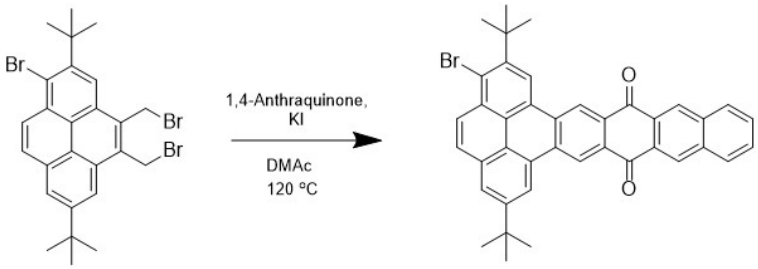

Synthesis of 1-bromo-2,7-di-t-butyl-4,5-pyrene-tetracenequinone (4): A 150 ml sealed-tube reactor was charged with 50 ml of dimethylacetamide, and the solvent was purged with N_2 for 30 minutes. 1-bromo-2,7-di-t-butyl-4,5-di-bromomethyl pyrene 3 (1.22 g, 2.10 mmol), 1,4-anthraquinone (1.75 g, 8.40 mmol), and potassium iodide (2.79 g, 16.8 mmol) were added, the tube was sealed, and the mixture was stirred at 120 °C for two days. The lid was then removed, and the mixture was stirred open to air for 1 hour. The mixture was allowed to cool to room temperature, poured into 200 ml of water, then filtered. The recovered solid was added to 100 ml of acetone, sonicated for 10 minutes, and then filtered. The solid was then added to 100 ml THF, sonicated for 10 minutes, and then filtered. The product was recovered as a light brown solid and used in the next step without further purification. *Yield: 0.81 g, 62%. *The mono-brominated compound was the main product, and thus was used to approximate yield.

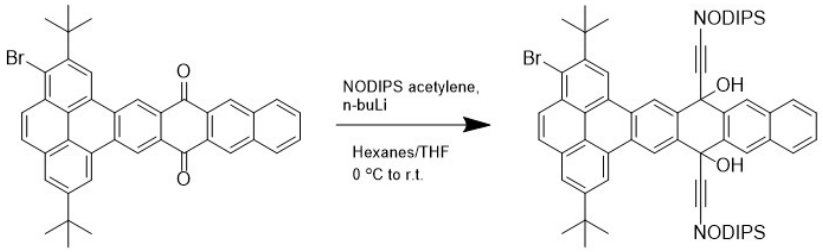

Synthesis of 1-bromo-TP-NODIPS-tetraol (5): A flame-dried 100 ml round bottom flask cooled under N_2 was charged with 20 ml of hexanes, NODIPS acetylene (1.21 g, 4.81 mmol) was added and the solution was cooled to 0 °C. 2.5 M n-butyllithium in hexanes (1.73 ml, 4.33 mmol) was added slowly, and the solution was stirred for 30 minutes. 1-bromo-2,7-di-t-butyl-4,5-pyrene-tetracenequinone **4** (0.300 g, 0.481 mmol) was added, and the mixture was stirred overnight at room temperature. The reaction was quenched with water, and the organic layer was washed with 10% aqueous HCl and water. The organic layer was dried with magnesium sulfate, and the solvent

removed. The product was purified via column chromatography in 6:1 hexanes:ethyl acetate to give the crude mixture of products as a dark red oil, which was carried directly to the next step.

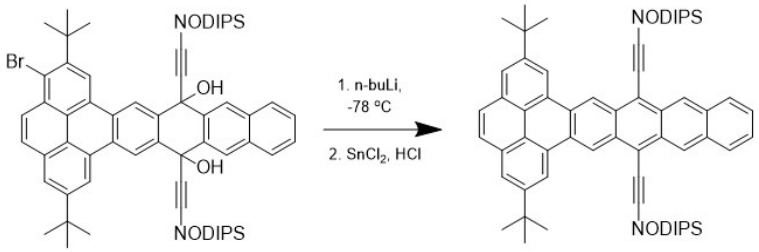

Synthesis of PT: 1-bromo-TP-NODIPS-tetraol **5** was dissolved in 2 ml DCM and added to a flame-dried 100 ml RB flask under N_2. The flask was then charged with 40 ml anhydrous THF and then cooled to -78 ^oC. 2.5 M n-butyllithium in hexanes (1.73 ml, 4.32 mmol, ~12 eq. to account for residual water and DCM) was then added dropwise. After stirring for 5 minutes, the reaction mixture was slowly quenched with 5 ml MeOH and allowed to warm to room temperature. Then, 0.500 g tin (II) chloride hydrate dissolved in ~2 ml of 10% aqueous HCl was added dropwise, and the mixture was stirred for 1 hr. The mixture was poured into water and extracted into diethyl ether. The organic layer was dried with magnesium sulfate, and after removal of the solvent was purified by column chromatography in 12:1 hexanes:DCM. Yield: 0.104 g, 20.8%. ^1H NMR (400 MHz, CDCl3): δ 10.07 (s, 2H), 9.45 (s, 2H), 9.16 (s, 2H), 8.15 (s, 2H), 8.06 (dd, J = 6.6, 3.2 Hz, 2H), 7.99 (s, 2H), 7.50 (dd, J = 6.6, 3.2 Hz, 2H), 1.76 (m, 4H), 1.70 (s, 18H), 1.53 (m, 4H), 1.44 (m, 4H), 1.40 (m, 28H), 1.28 (m, 4H), 1.21 (m, 8H), 1.05 (q, J = 8.4 Hz, 4H), 0.80 (t, J = 6.8 Hz, 6H). HRMS (APCI with direct probe injection) for [M+1]+: calc. For $C_{72}H_{94}Si_2$: 1014.6894, found: 1014.6870.

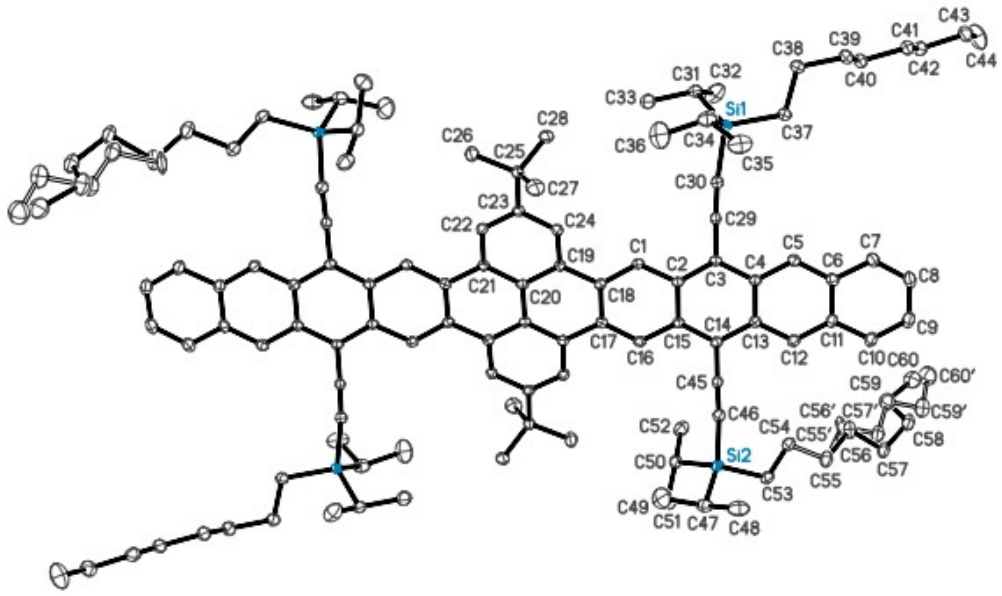

Figure S2 Crystal structure for **TPT**.

^{1}H NMR Spectra

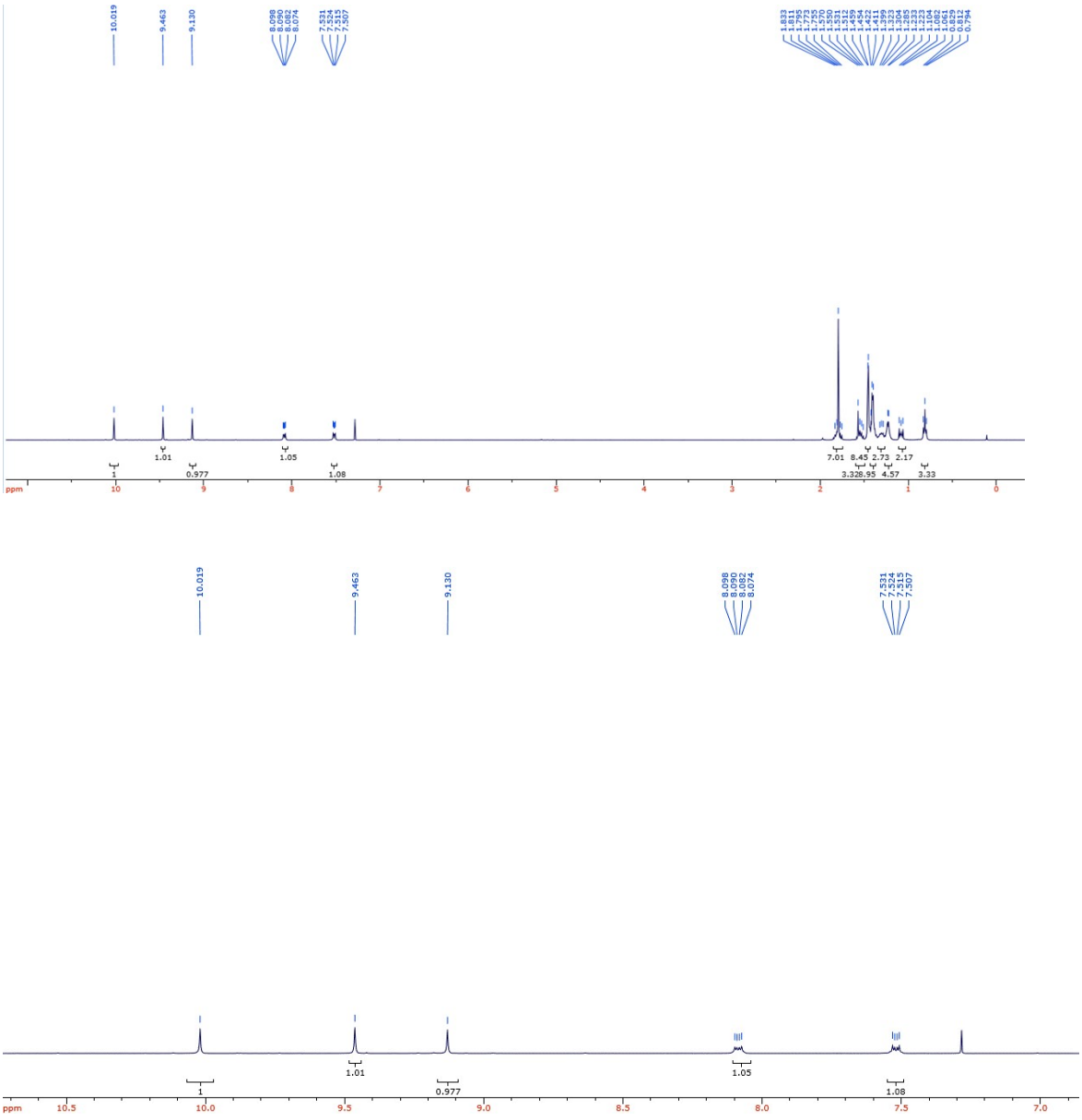

Figure S3 **TPT** ^{1}H NMR.

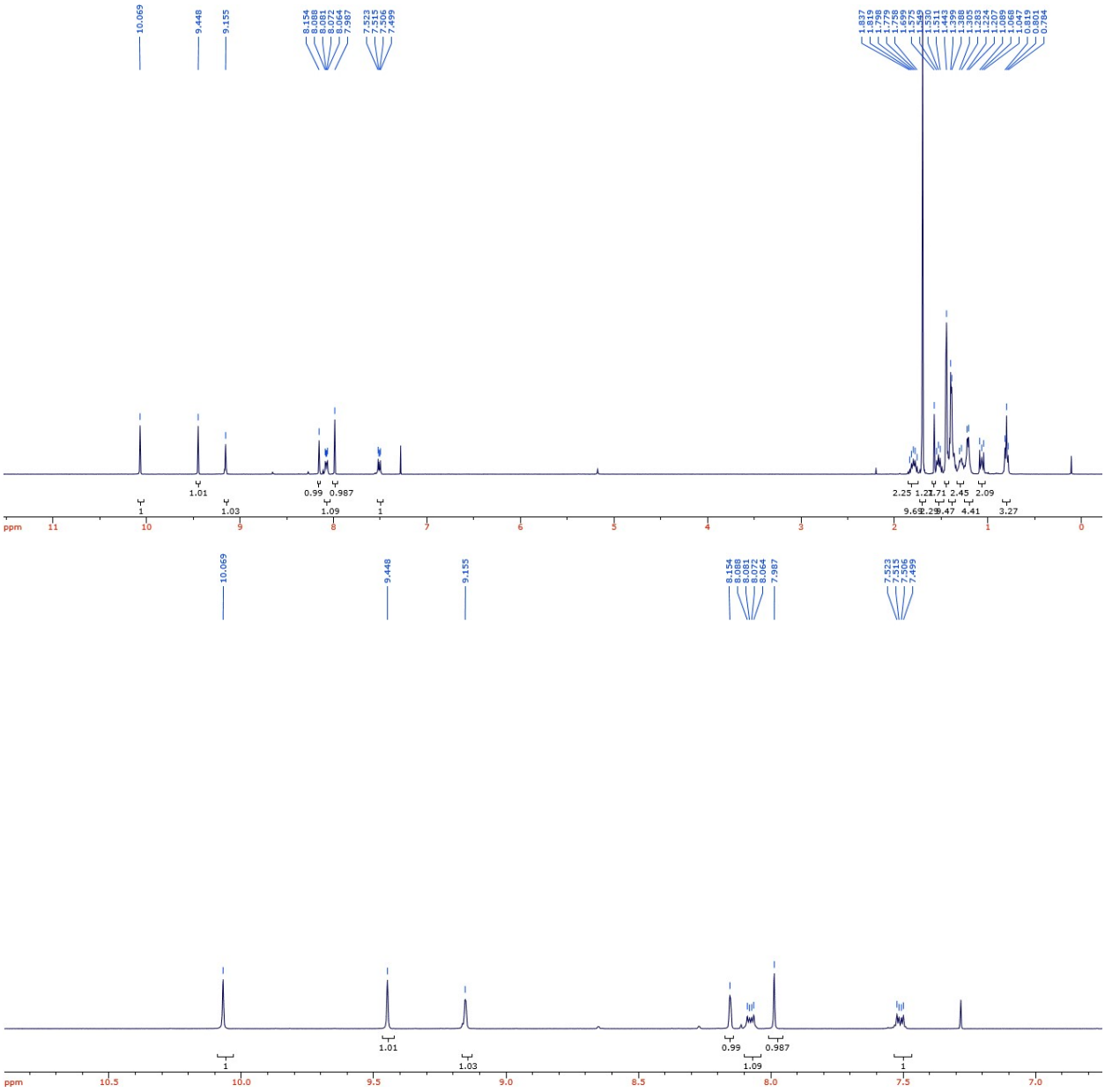

Figure S4 **PT** ^{1}H NMR.

Calculated Excited States

Electronic excited states were investigated via linear response time-dependent density functional theory (TDDFT). The long-range corrected functional LC-ωHPBE was used along with Def2TZVP basis set as implemented in Gaussian 16 (version C.01).[3–6] The range-separation parameter ω was tuned by minimizing the sum of the ionization energy and the highest occupied molecular orbital (HOMO) energy,[7,8] as used in a recent study of the similar system.[1] Excited state analyses, including natural transition orbitals, fragment charge transfer matrix, and transition density visualization, were performed using Multiwfn (version 3.8_dev).[9]

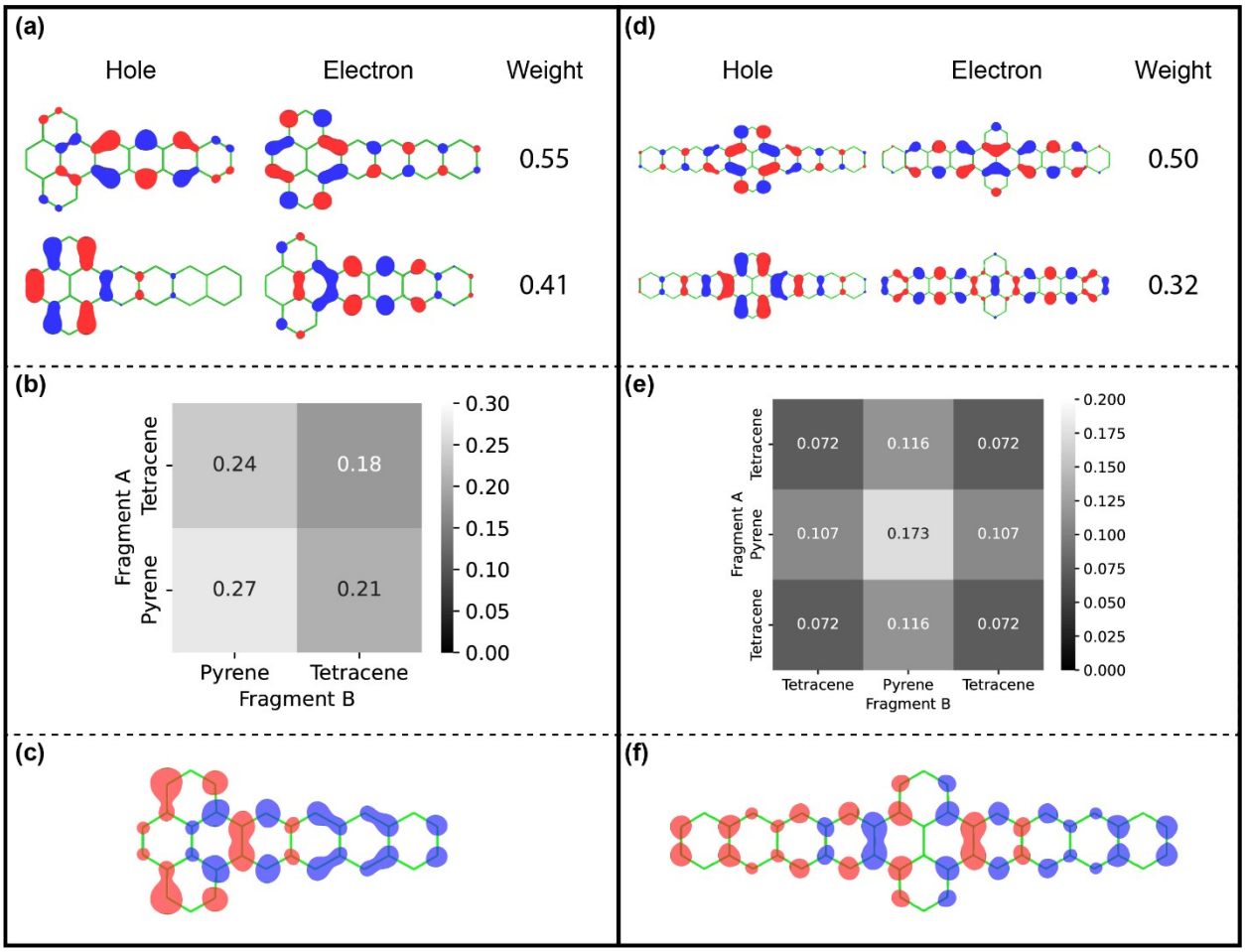

Figure S5. Major natural transition orbitals (isovalue 0.03 e/Å3) of the excitation around 390 nm for **PT** (a) and **TPT** (d). Fragment charge transfer matrix for **PT** (b) and **TPT** (e), where two or three fragments are defined by group the 16 carbon atoms in pyrene as one fragment and the rest carbon atoms as one or two tetracene fragments. Transition densities (isovalue 0.003e) for **PT** (c) and **TPT** (f).

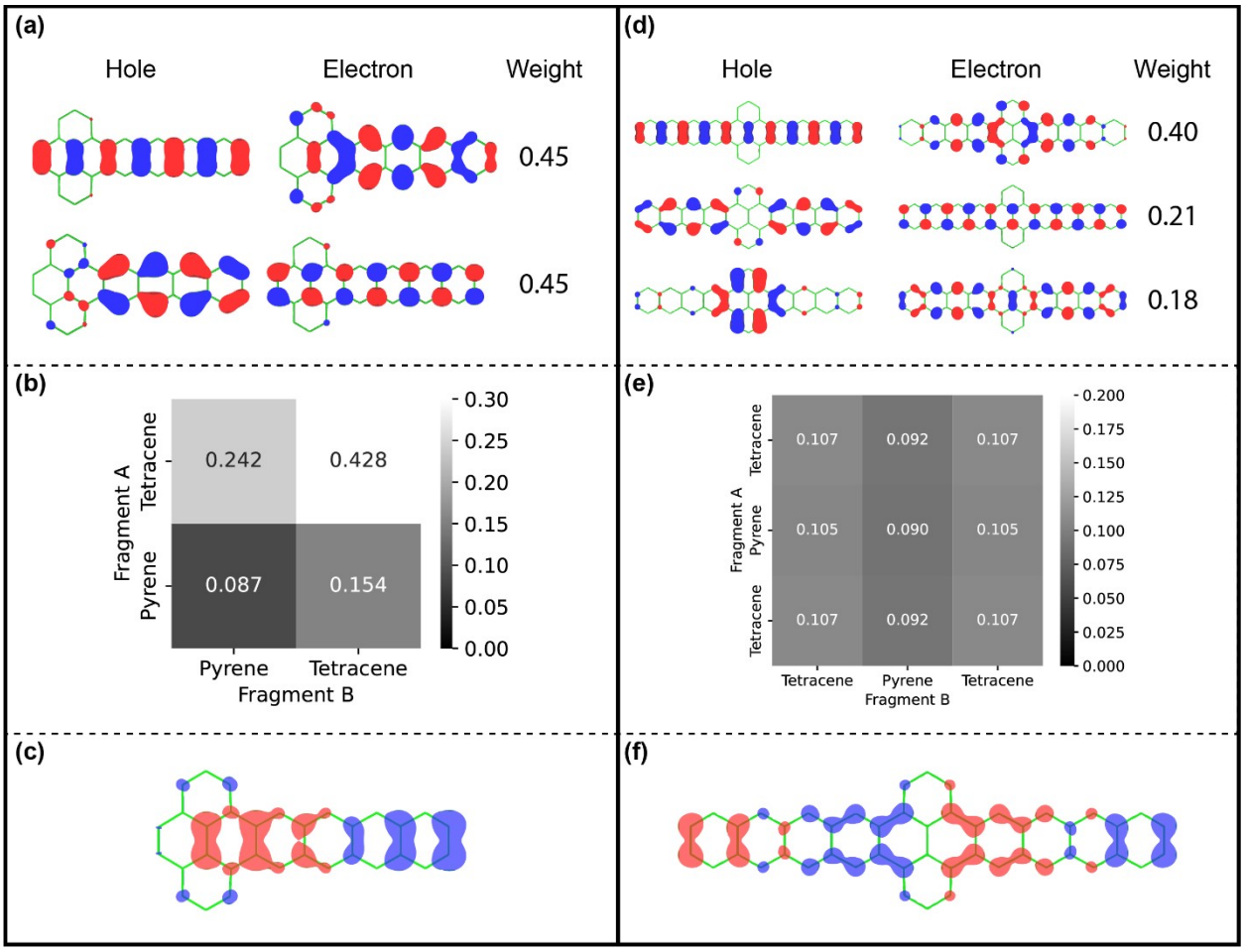

Figure S6. Major natural transition orbitals (isovalue 0.03 e/Å3) of the excitation around 315 nm for **PT** (a) and **TPT** (d). Fragment charge transfer matrix for **PT** (b) and **TPT** (e), where two or three fragments are defined by group the 16 carbon atoms in pyrene as one fragment and the rest carbon atoms as one or two tetracene fragments. Transition densities (isovalue 0.003e) for **PT** (c) and **TPT** (f).

Optical Spectroscopy Methods

Coherent Libra Ti:Sapphire laser outputs pulses centered at 800 nm with repetition rate of 1kHz, ~ 4 W power and ~ 100 fs pulse width. The 800 nm beam splits into two pathways: One TOPAS, a commercial optical parametric amplifier, at right phase-matching angle, a pulse centered at 600 nm is generated as our pump beam to the sample. The other beam was directed to a Ti:Sapphire crystal with different thickness to generate 450 nm-850 nm and 750 nm-1600 nm probe light. The delay time between the pump beam and the probe beam is controlled by the multipath delay stage for fsTA, which can reach up to ~ 5 ns delay time. As for nsTA, the longer delay time is manipulated electronically with EOS (electro-optical system). For both nsTA and fsTA, the broadband probe beam is separated into two beams for reference

detection to minimize the influence of pulse-to-pulse fluctuation to the transient absorption signal and increase the signal quality. Each beam is focused to the optical fibers and detected by the photodiode array in Ultrafast system. For low temperature TA measurements, the sample is mounted on an Oxford Instruments nitrogen vapor cryostat. The solution sample was prepared in the glovebox with a concentration of 2.2 μM in 2-MeTHF.

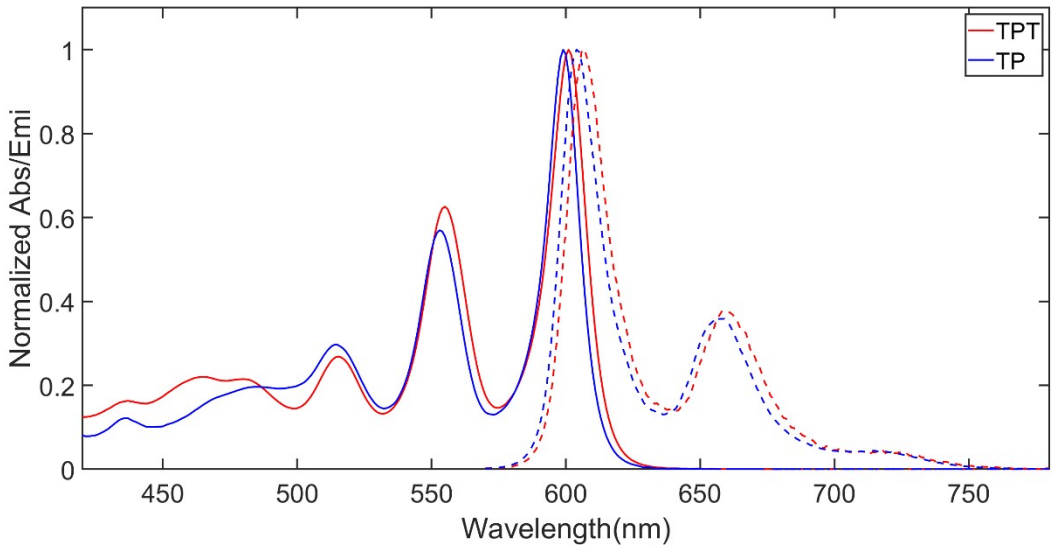

Figure S7. Normalized absorption and emission spectra for **TPT** and **PT** in 2-MeTHF at room temperature. The solid red line is the absorption spectrum of **TPT**, and the dashed red line is the emission spectrum of **TPT**. The solid (dashed) blue line is the absorption (emission) spectrum of **PT**.

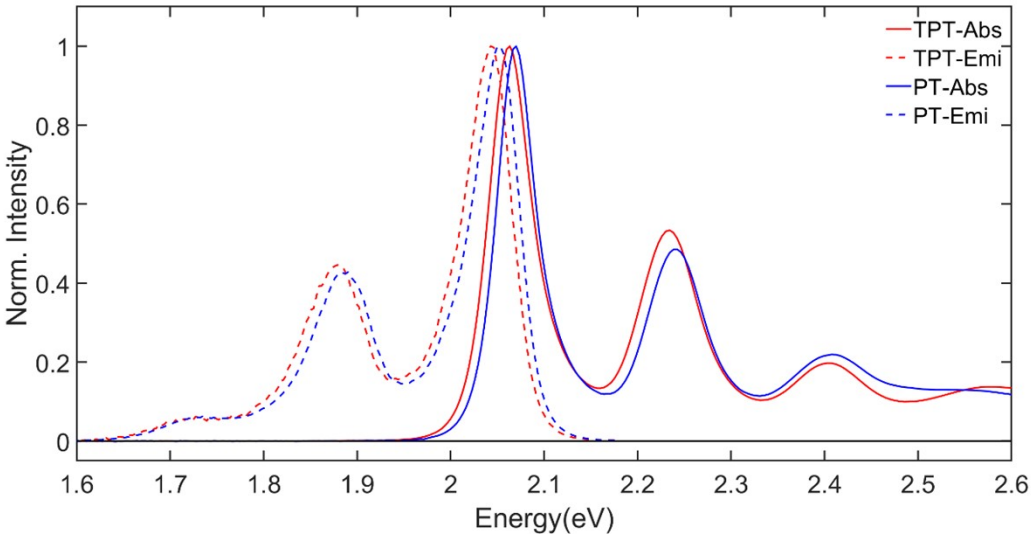

Figure S8. Jacobian corrected normalized absorption and emission spectra for **TPT** and **PT** in 2-MeTHF at room temperature. The solid red line is the absorption spectrum of **TPT**, and the dashed red line is the emission spectrum of **TPT**. The solid (dashed) blue line is the absorption (emission) spectrum of **PT**.

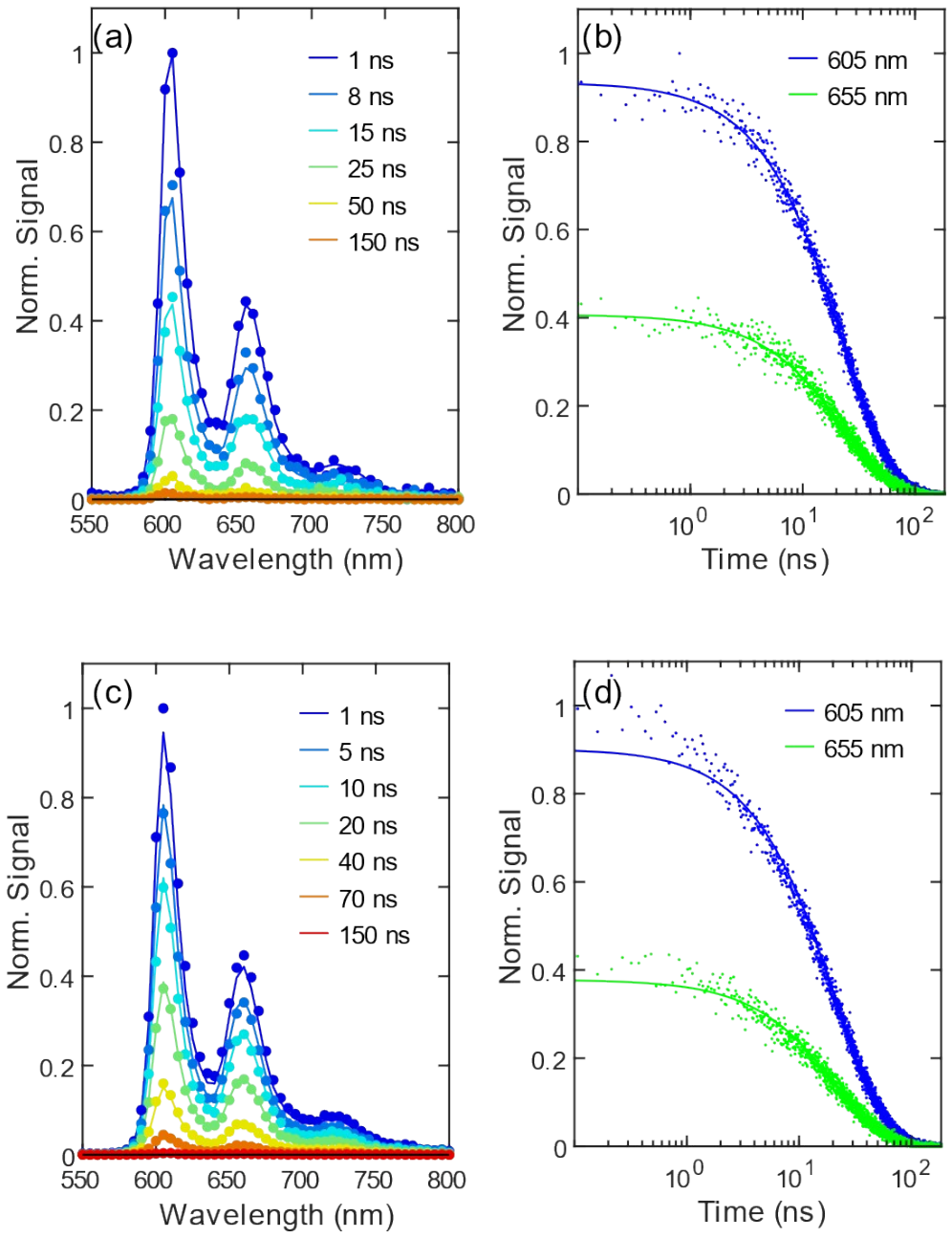

Figure S9 (a) TCSPC for **PT** in 2-MeTHF at selected delay times at room temperature. (b) TCSPC for **PT** in 2-MeTHF at the selected peak wavelengths at room temperature. (c) TCSPC for **TPT** in 2-MeTHF at selected delay times at room temperature. (d) TCSPC for **TPT** in 2-MeTHF at the selected peak wavelengths at room temperature.

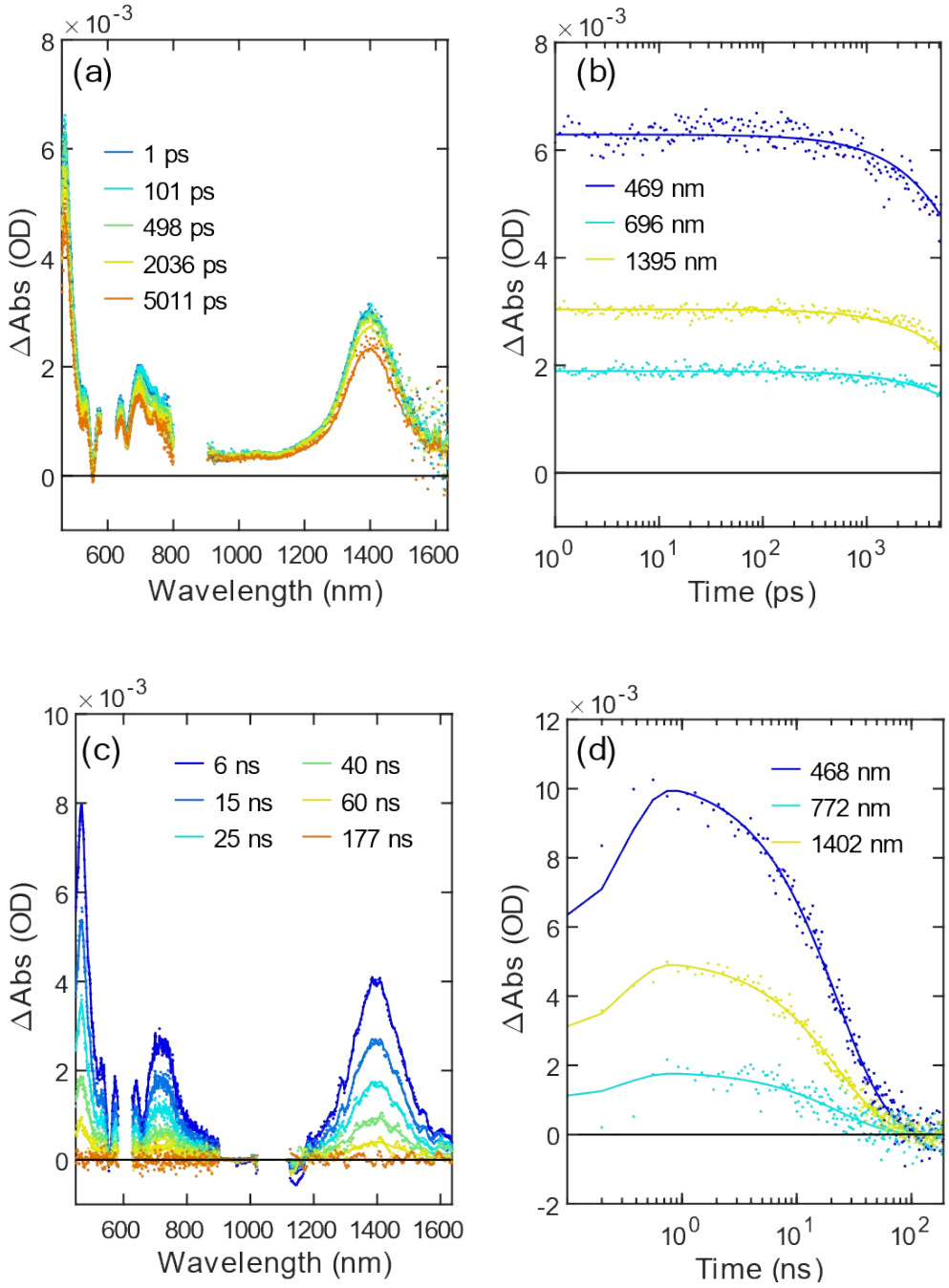

Figure S10 (a) fsTA spectra for **PT** in 2-MeTHF at the selected delay times at room temperature. (b) Kinetic traces at selected wavelengths from (a). (c) nsTA for **PT** in 2-MeTHF at the selected delay times at room temperature. (d) Kinetic traces at selected wavelengths from (c).

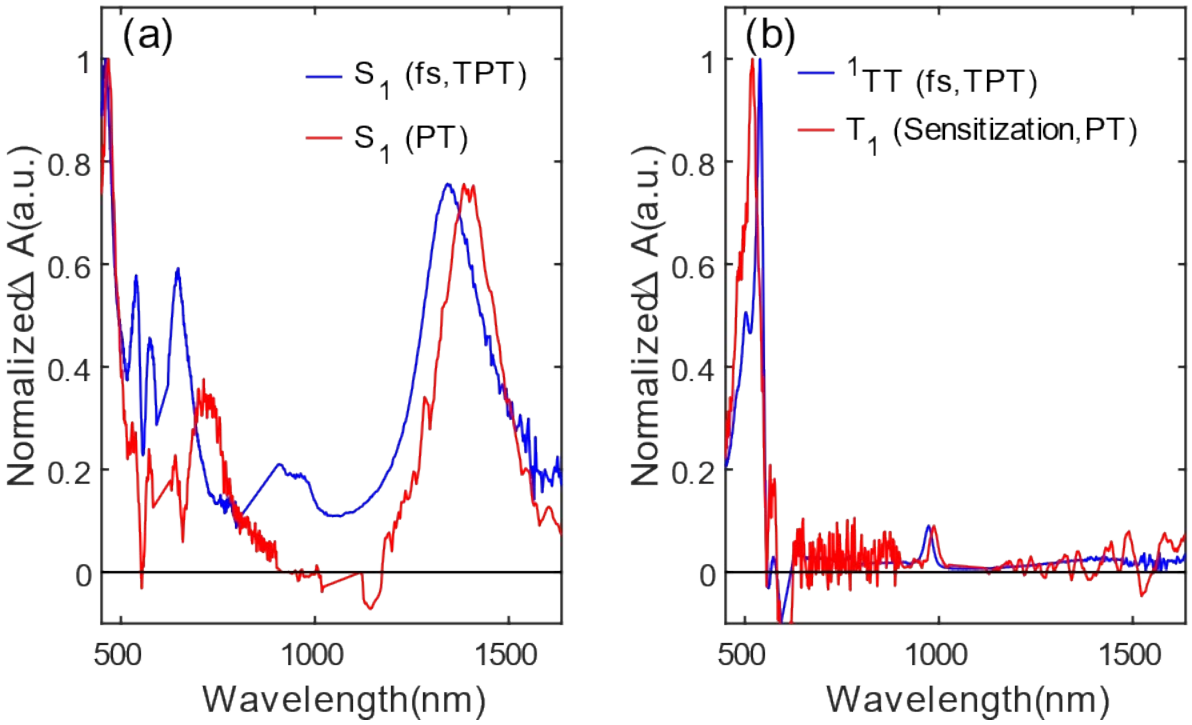

Figure S11 (a) Normalized species associate spectra for S_1 from fsTA measurement on **TPT** in 2-MeTHF at room temperature (blue) and for S_1 from nsTA measurement on **PT** in 2-MeTHF at room temperature (red). (b) Normalized species associate spectra for ^{1}TT from fsTA measurement on **TPT** in 2-MeTHF at room temperature (blue) and for T_1 from nsTA measurement on PT/anthracene in toluene at room temperature (red).

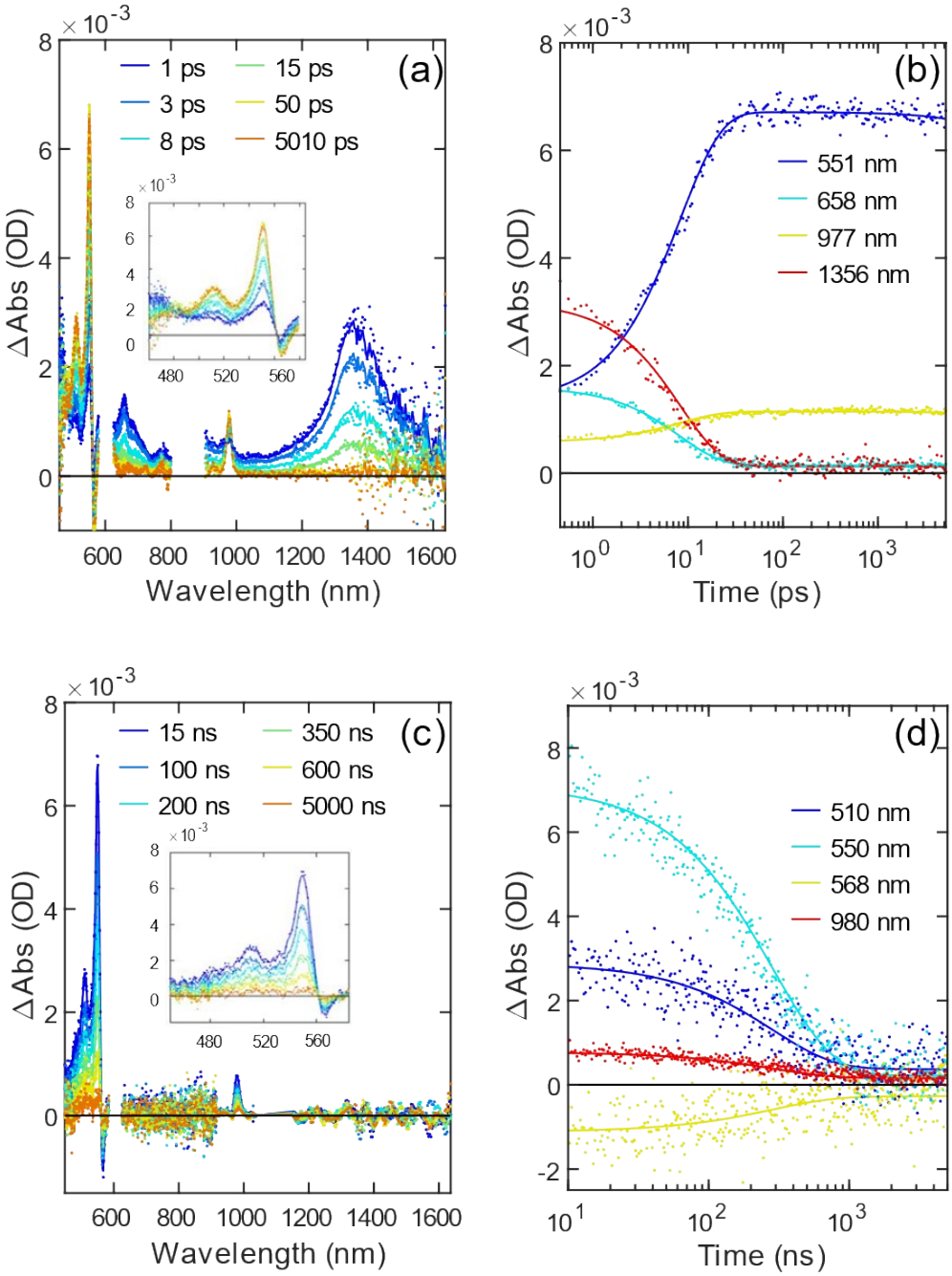

Figure S12 (a) The selected delay times for fsTA spectra of **TPT** in 2-MeTHF at 77K. The wavelength ranges from 450 nm to 1650 nm. (b) Kinetic traces at selected wavelengths from (a). (c) The selected delay times for nsTA spectra of **TPT** in 2-MeTHF at 77K. The wavelength ranges from 450 nm to 1650 nm. (d) Kinetic traces at selected wavelengths from (c).

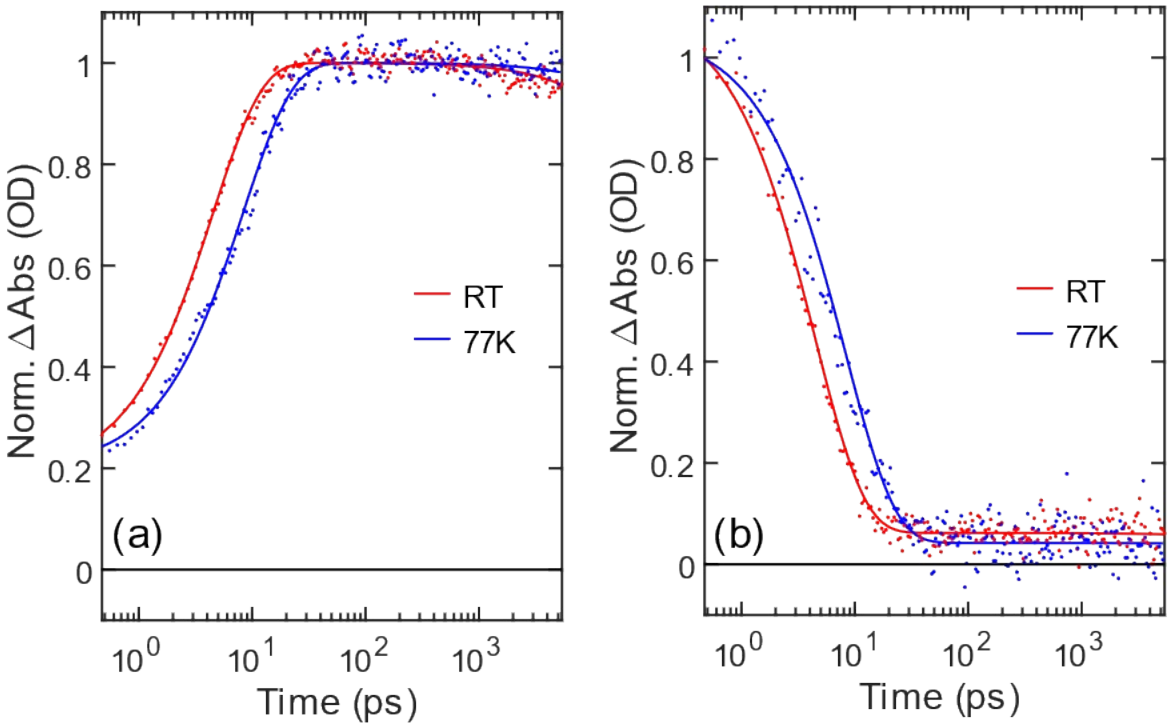

Figure S13 (a) The normalized kinetic traces for **TPT** in 2-MeTHF at RT and 77K at 540 nm and 550 nm, respectively. (b) The normalized kinetic traces for **TPT** in 2-MeTHF at RT and 77K at 1345 nm and 1356 nm, respectively.

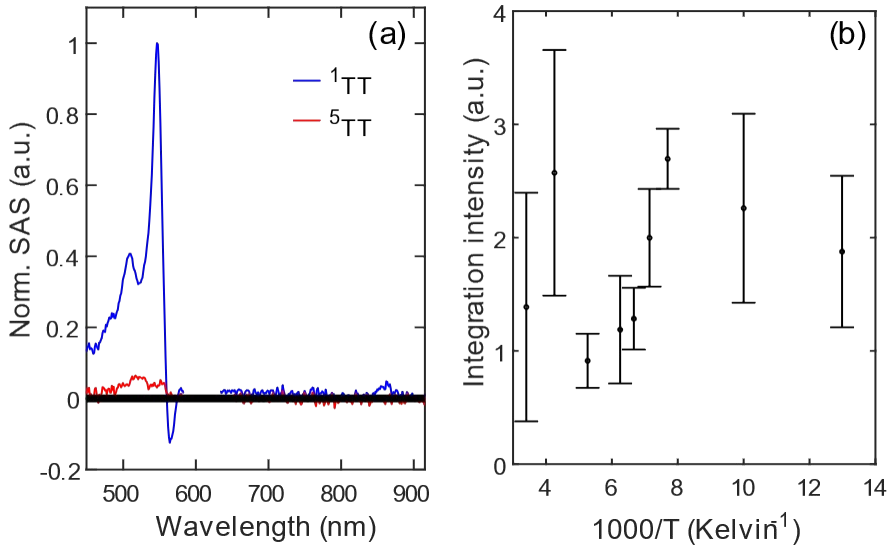

Figure S14 (a) Normalized species associated spectra (SAS) for ^{1}TT and ^{5}TT from nsTA on **TPT** in 2-MeTHF at 130 K. (b) The integrated intensity of ^{5}TT SAS spectra over the temperatures. The integration range is from 460 nm to 570 nm.

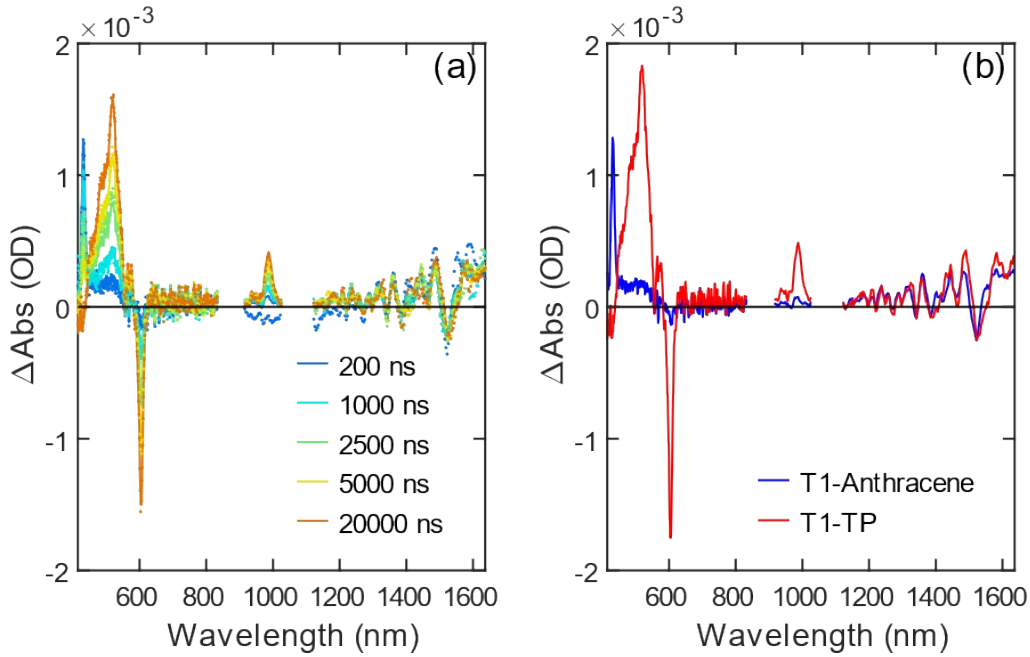

Figure S15 (a) **PT** sensitization with anthracene in toluene at room temperature in the selected wavelengths. (b) Species associated spectra for the T_1 spectra of anthracene and **PT**.

TREPR spectroscopy

The TREPR data was collected at X-band with Bruker ELEXSYS E580 in transient mode, followed by optical excitation from the optical parametric oscillator (OPO Radiant SE 355LD), centered at 600 nm (10Hz repetition rate, 3.5 mJ/pulse, 5 ns FWHM). The system is equipped with dielectric resonator (Bruker ER4118 X-MS3, Q=500 and EN4118X-MD4, Q=2500) and coupled with the closed cycle helium cryostat (Bruker/Cold Edge Technologies) to cool down the sample to the desired temperatures. The attenuation of the CW microwave power is 17 dB, which gives microwave power 2.99 mW. The concentration of the **TPT** sample was prepared to be 67 uM in 2-MeTHF inside the N_2 glovebox. The solution sample in the EPR tube was degassed with several freeze-pump-thaw cycles followed by fame-sealing process under vacuum with oxyhydrogen torch.

Pulsed EPR

The pulsed EPR data was collected with Bruker ELEXSYS E580 in pulse mode and equipped with dielectric resonator, Bruker ER4118 X-MS3. The experiment is performed at 10K to avoid fast spin relaxation. The microwave frequency is centered at 9.35 GHz. The transient

nutation traces are obtained with a pulse sequence of $P_{nut} - T - \frac{\pi}{2} - \tau - \pi$, where P_{nut} is variable, T is 300 ns, τ is 148 ns, π pulse length is 12 ns with microwave power set to be 20 dB, which is optimized to the ideal tuning angle for the quintet spin echo. The T_2 traces are measured with Hann Echo sequence of $\frac{\pi}{2} - \tau - \pi - \tau - echo$, where τ is variable and the π pulse length is 12 ns. The echo-detected field-swept EPR spectrum in Q band is measured with Q-band EN5107D2 resonator.

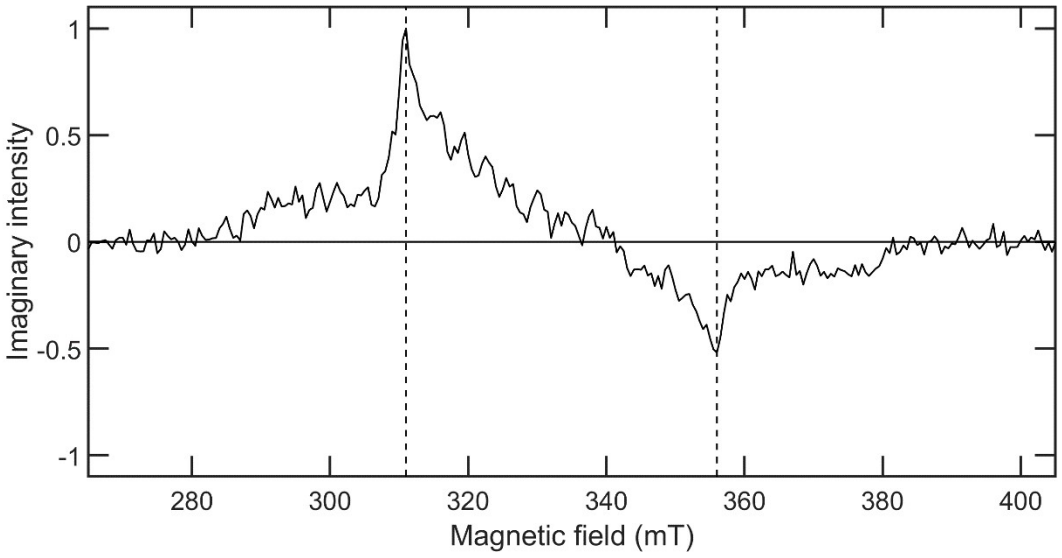

Figure S16 The normalized intersystem crossing EPR spectrum of **PT** in a heavy atom solvent (4:1 toluene: 1-iodobutane), formed upon photoexcitation at 600 nm at 76K. The two vertical dashed lines located at the two peaks are located at 311 mT and 356 mT, respectively.

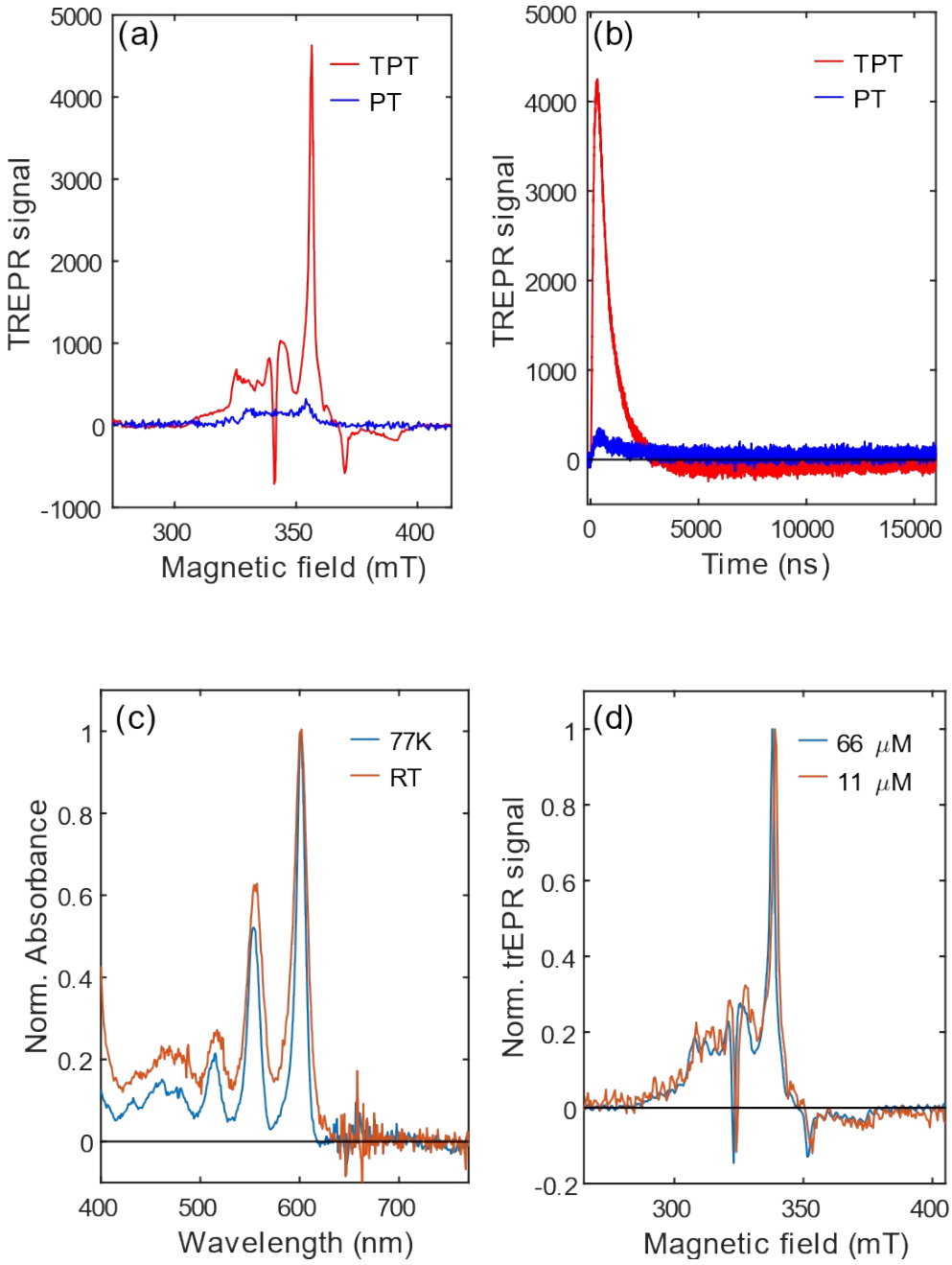

Figure S17 (a) EPR spectrum for **TPT** (red) and **PT** (blue) in 2-MeTHF at 76K, selected at peak signal delay time. Concentrations of **TPT** and **PT** are 66 μM and 220 μM, respectively. (b) Kinetic traces for **TPT** (red) and **PT** (blue) at 356 mT. (c) UVVis spectra for **TPT** in 2-MeTHF at 77K (blue) and room temperature (red) with concentration of 66 μM. (d) EPR spectra for **TPT** in 2-MeTHF at 77K for concentrations of 66 μM (blue)and 11 μM (red).

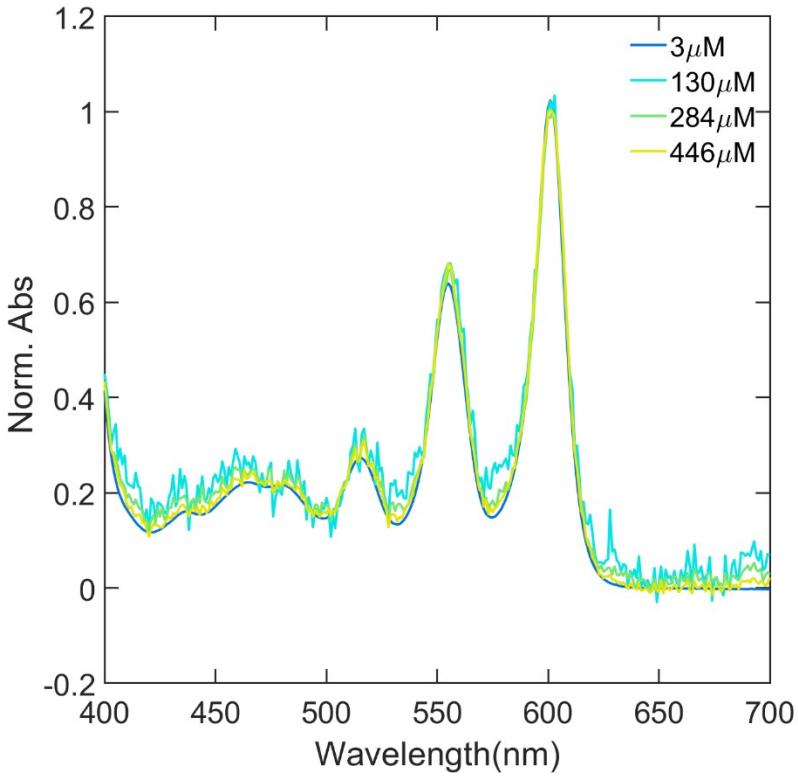

Figure S18. Normalized steady state absorption spectra for **TPT**/2-MeTHF at four different concentrations at room temperature.

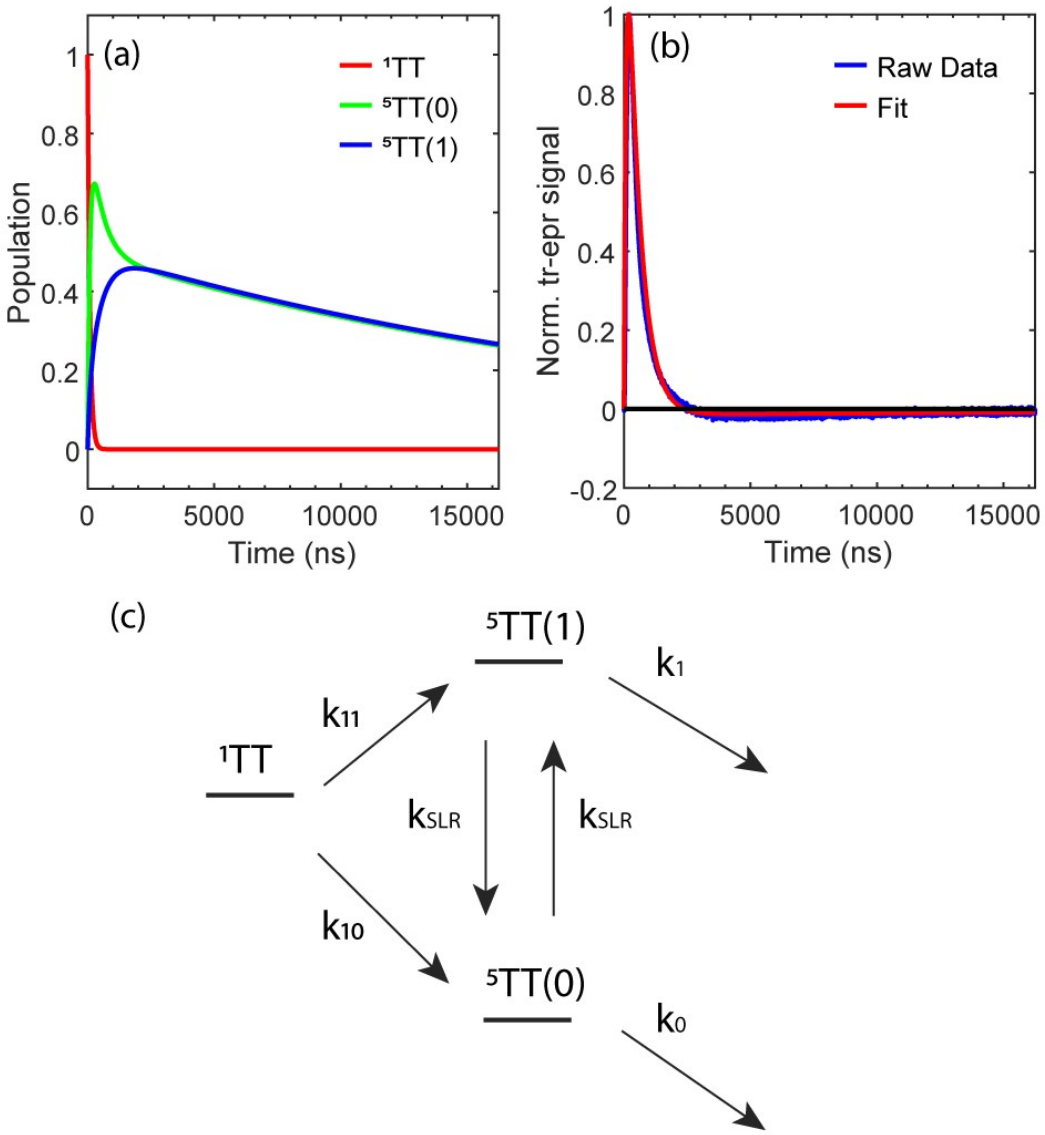

Figure S19 (a) Population analysis for ^{1}TT, ^{5}TT(1) and ^{5}TT(0) based on the kinetic scheme shown in (c). (b) The fit of ordinary differential equation to kinetic trace at 338 mT for TREPR at 76K. τ_{11}, τ_{10}, τ_{SLR}, τ_1, and τ_0 are 106.6 ns, 446.3 ns, 2 μs, 19.1 μs, and 38.4 μs, respectively. (c) Kinetic scheme for **TPT** singlet fission measured with TREPR at 76K.

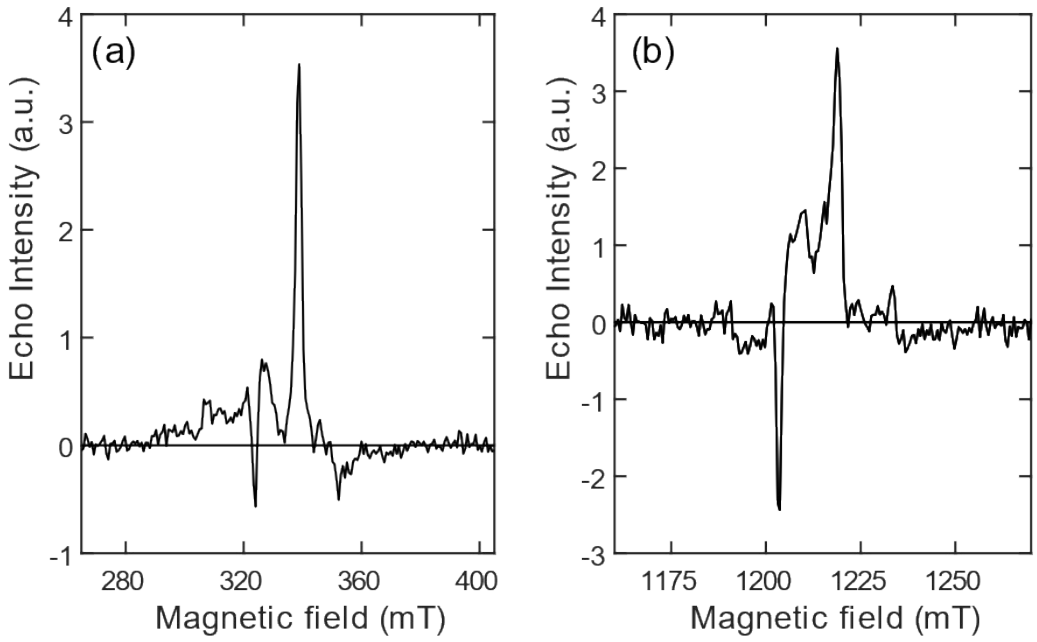

Figure S20 (a) Echo-detected field-swept EPR spectrum for **TPT**/2-MeTHF measured at 10K in X band. (b) Echo-detected field-swept EPR spectrum for **TPT**/2-MeTHF measured at 10K in Q band.

Kinetic simulation

Based on the kinetic scheme shown in Figure 7, we construct the following rate equations accordingly.

$$\frac{dS_1}{dt} = -(k_{fiss} + k_r)S_1 + k_{fus}{}^1TT$$

$$\frac{d^1TT}{dt} = k_{fiss}S_1 - (k_{fus} + k_{1TT})^1TT$$

$$\frac{d^5TT}{dt} = k_{SQ}{}^1TT - k_{5TT}{}^5TT$$

We solve the differential equations above with the built-in function, ode15s, in MATLAB. The initial population of S_1, ^{1}TT and ^{5}TT are set to be 1, 0, and 0, respectively. k_{fiss} and k_{fus} are determined by the lifetime measured in fsTA and the emission quantum yield. Since $k_{fiss} + k_{fus} = k_{measured,fs}$ $(1/\tau_{fs})$[10] and $\Phi_{Emi} = \frac{k_{fus}}{k_{fiss}}$, k_{fiss} is calculated to be $k_{measured,fs} \times (1-\Phi_{Emi})$ and k_{fus} is

$k_{measured,fs} \times \Phi_{Emi}$. We obtain k_r by measuring τ_r with TCSPC and assuming 100% Φ_{Emi}. k_{1TT} and k_{SQ} are attributed to the nsTA ^{1}TT ESA decay lifetime, $\tau_{ns,1TT}$. We tune the branching ratio[10] between k_{1TT} and k_{SQ} until the ratio of ^{5}TT to ^{1}TT populations are about the normalized SAS amplitude of ^{5}TT, ~ 5%. Because ^{5}TT signal is too weak, we can only get the lower bound of k_{5TT} to be < 2.9×10^4 sec^{-1}. k_{5TT} are both set to be 2.9×10^4 sec^{-1} for room temperature and 77K for the kinetic simulation. The time-dependent population analysis can be seen in Figure S13 for both room temperature and 77K.

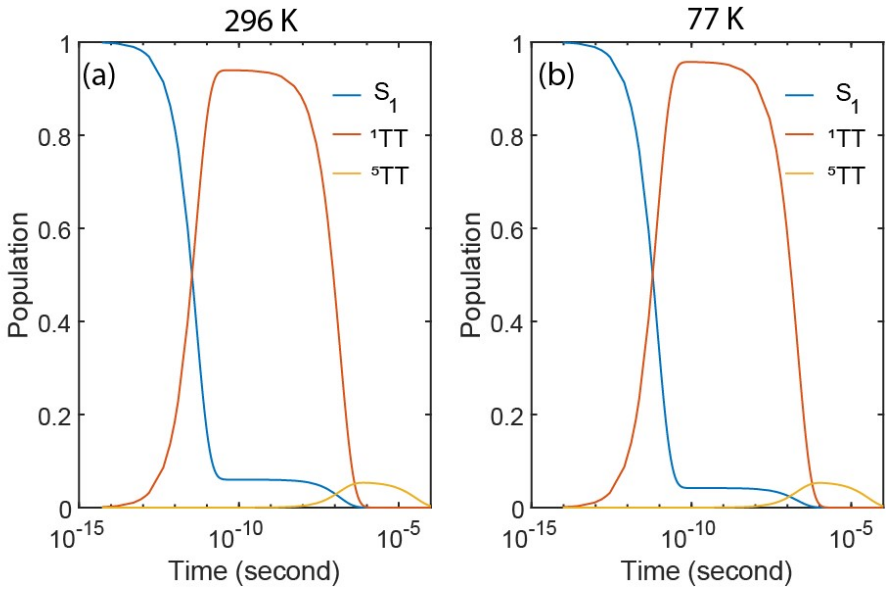

Figure S21 Normalized population for S_1, ^{1}TT, and ^{5}TT states from our kinetic model simulation shown in Figure 7 at room temperature for (a) and 77K for (b).

Exchange energy calculations

Considering angular momentum coupling between the two triplet states, we can approximate the interaction with Heisenberg Hamiltonian,

$$H = JS_A \cdot S_B = J(S_A + S_B)^2 - {S_A}^2 - S_B$$

, where A and B represent the two chromophores in the dimer, which is the isotropic term in spin exciton Hamiltonian introduced in the main text. The energetics of the three spin states ^{1}TT, ^{3}TT (three states), and ^{5}TT (five states) are -2*J*, -*J*, and *J*, respectively. The wavefunctions of the nine

states can be constructed with Clebsch-Gordan coefficient and spin quantum number (m_s) on each chromophore A and B,

$$|^1TT_0\rangle = \frac{1}{\sqrt{3}}(|00\rangle - |+\ -\rangle - |-\ +\rangle)$$

$$|^3TT_0\rangle = \frac{1}{\sqrt{2}}(|+-\rangle - |-\ +\rangle)$$

$$|^3TT_{\pm}\rangle = \frac{1}{\sqrt{2}}(|\pm 0\rangle - |0\pm\rangle)$$

$$|^5TT_0\rangle = \frac{1}{\sqrt{6}}(2|00\rangle + |+-\rangle + |-\ +\rangle)$$

$$|^5TT_{\pm 1}\rangle = \frac{1}{\sqrt{2}}(|\pm 0\rangle + |0\pm\rangle)$$

$$|^5TT_{\pm 2}\rangle = |\pm\ \pm\rangle.$$

As we can see, all the (TT) are multi-determinantal states except for $|^5TT_{\pm 2}\rangle$. Since in Density Functional Theory (DFT), only energetics of the single determinant can be calculated, here, we begin the calculation from $|^5TT_{\pm 2}\rangle$. To calculate *J*, we use broken symmetry DFT (BS-DFT) to get E_{BS}, and compare the energy difference between E_{BS} and energetics of $|^5TT_{\pm 2}\rangle$ (E_{HS}) for *J*. The localized four singly occupied molecular orbitals (SOMO) for $|^5TT_{\pm 2}\rangle$ are shown in Figure S11, assuming they are all spin-up. By flipping down the spin of orbital b and d and calculating the single point energy, we get E_{BS}. Based on the Heisenberg Hamiltonian and given the E_{BS} and E_{HS} together with the corresponding spins, we can calculate *J* with

$$J = 2\frac{E_{HS} - E_{BS}}{\langle S^2\rangle_{HS} - \langle S^2\rangle_{BS}}$$

, and the calculated value for the different dimers can be shown in Table S1. The geometry is optimized with ωb97XD[11]/6-31G(D) in Gaussian 09[12]. The energetics and the spins are calculated with the same calculation method and basis set in pyscf[13–15]. We also compare the *J* from BS-DFT

with the literature, which reports the *J* values calculated with RAS-SF method[16]. Although the absolute values don't match very well, both sign and relative magnitude from BS-DFT align with that from RAS-SF method.

Table S1. Exchange energy comparison for different SF dimers. Nomenclature for dimers other than TPT comes from Reference 16, with m and p signifying meta and para connections, respectively, through the phenyl bridge.

Unit: GHz	Broken symmetry DFT	RAS_SF
Bm_PC	-3675	-371
Bp_PC	10107	3405
Bm_TA	-100	-7
Bp_TA	283	70
TPT	-512	NA

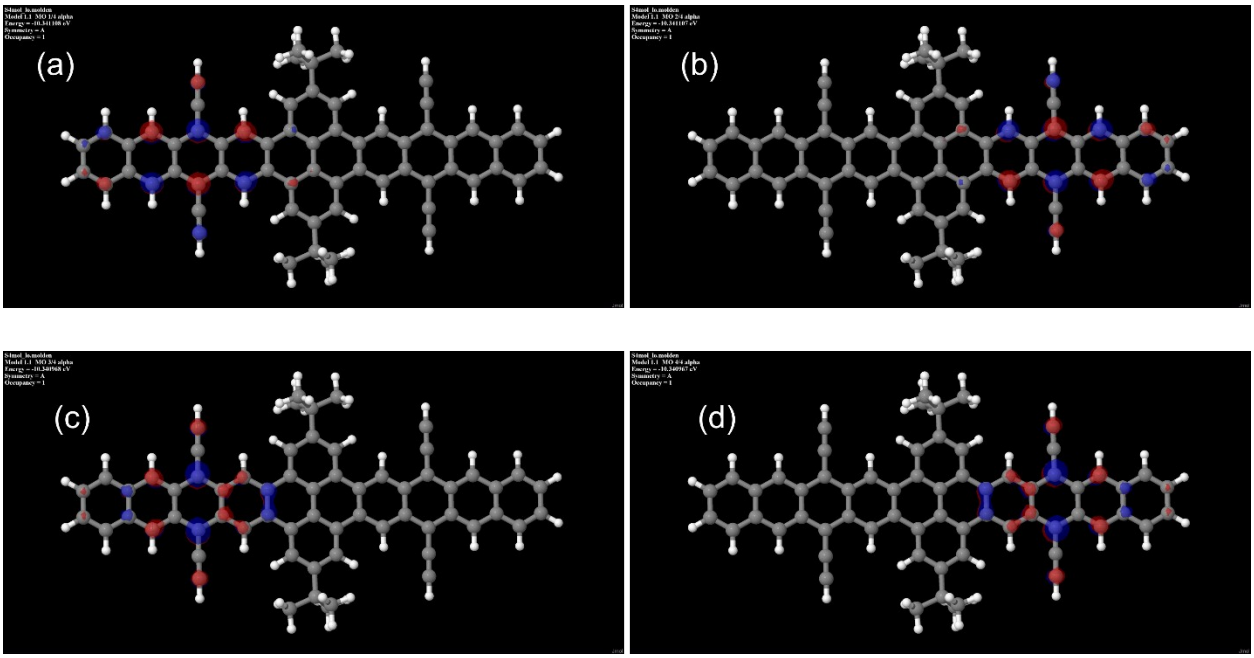

Figure S22 The localized molecular orbitals of the four SOMO for $|^5TT_{\pm 2}\rangle$.

Reference

1. Ai, Q. *et al.* Nanoribbons or weakly connected acenes? The influence of pyrene insertion on linearly extended ring systems. *J. Mater. Chem. C* **9**, 16929–16934 (2021).
2. Kumarasamy, E. *et al.* Properties of Poly- and Oligopentacenes Synthesized from Modular Building Blocks. *Macromolecules* **49**, 1279–1285 (2016).
3. Frisch, M. J. *et al.* Gaussian 16 Rev. C. 01, 2016. (2016).
4. Weigend, F. & Ahlrichs, R. Balanced basis sets of split valence, triple zeta valence and quadruple zeta valence quality for H to Rn: Design and assessment of accuracy. *Phys. Chem. Chem. Phys.* **7**, 3297 (2005).

5. Henderson, T. M., Izmaylov, A. F., Scalmani, G. & Scuseria, G. E. Can short-range hybrids describe long-range-dependent properties? *The Journal of Chemical Physics* **131**, 044108 (2009).
6. Vydrov, O. A. & Scuseria, G. E. Assessment of a long-range corrected hybrid functional. *The Journal of Chemical Physics* **125**, 234109 (2006).
7. Stein, T., Kronik, L. & Baer, R. Prediction of charge-transfer excitations in coumarin-based dyes using a range-separated functional tuned from first principles. *The Journal of Chemical Physics* **131**, 244119 (2009).
8. Sun, H. *et al.* Ionization Energies, Electron Affinities, and Polarization Energies of Organic Molecular Crystals: Quantitative Estimations from a Polarizable Continuum Model (PCM)-Tuned Range-Separated Density Functional Approach. *J. Chem. Theory Comput.* **12**, 2906–2916 (2016).
9. Lu, T. & Chen, F. Multiwfn: A multifunctional wavefunction analyzer. *J. Comput. Chem.* **33**, 580–592 (2012).
10. Pogliani, L. & Terenzi, M. Matrix formulation of chemical reaction rates: A mathematical chemical exercise. *J. Chem. Educ.* **69**, 278 (1992).
11. Chai, J.-D. & Head-Gordon, M. Long-range corrected hybrid density functionals with damped atom–atom dispersion corrections. *Phys. Chem. Chem. Phys.* **10**, 6615 (2008).
12. M. J. Frisch *et al.* Gaussian 09, Revision A.02. (2016).
13. Sun, Q. *et al.* Recent developments in the P Y SCF program package. *J. Chem. Phys.* **153**, 024109 (2020).

14. Qiming Sun, Timoth C. Berkelbach, Nick S. Blunt, George H. Booth, & Garnet Kin-Lic Chan. PySCF: the Python-based simulations of chemistry framework. *WIREs Comput Mol Sci* 8:e1340 (2018).

15. Sun, Q. Libcint: An efficient general integral library for Gaussian basis functions. *J. Comput. Chem.* **36**, 1664–1671 (2015).

16. Abraham, V. & Mayhall, N. J. Simple Rule To Predict Boundedness of Multiexciton States in Covalently Linked Singlet-Fission Dimers. *J. Phys. Chem. Lett.* **8**, 5472–5478 (2017).